

# Statistical Physics of Design

Andrei A. Klishin,<sup>1,2</sup> Colin P.F. Shields,<sup>3</sup> David J. Singer,<sup>3</sup> and Greg van Anders<sup>1,2</sup>

<sup>1</sup>*Department of Physics, University of Michigan, Ann Arbor, Michigan 48109, USA*

<sup>2</sup>*Center for the Study of Complex Systems, University of Michigan, Ann Arbor, Michigan 48109, USA*

<sup>3</sup>*Naval Architecture and Marine Engineering, University of Michigan, Ann Arbor, Michigan 48109, USA*

(Dated: May 14, 2018)

A key challenge in complex design problems that permeate science and engineering is the need to balance design objectives for specific design elements or subsystems with global system objectives. Global objectives give rise to competing design pressures, whose effects can be difficult to trace in subsystem design. Here, using examples from arrangement problems, we show that the systems-level application of statistical physics principles, which we term “systems physics”, provides a detailed characterization of subsystem design in terms of the concepts of stress and strain from materials physics. We analyze instances of routing problems in naval architectures, and show that systems physics provides a direct means of classifying architecture types, and quantifying trade-offs between subsystem- and overall performance. Our approach generalizes straightforwardly to design problems in a wide range of other disciplines that require concrete understanding of how the pressure to meet overall design objectives drives the outcomes for component subsystems.

## I. INTRODUCTION

Designing products with an emergent, overall function that is more than the sum of their parts is a crucial challenge in science and engineering.[1] Meeting this challenge is complicated by the fact that, for many complex products,[2–6] different subsystems employ diverse technologies and are designed using a variety of methodologies. Moreover, meeting the overall design goal for a specific product is seldom achieved by optimal performance for every individual subsystem.[7] The need to design subsystems that achieve target performance and contribute to overall system outcomes is becoming more pressing.[8, 9] The increased pressure arises because engineered products in a wide variety of industries now incorporate several distinct, but interconnected types of functionality.[8] As a result, for many modern engineered products more economic value is added in designing a product than in manufacturing it.[9] Making design more effective requires the ability to understand and quantify how the design of a subsystem is affected by overall design objectives, and how deviations from optimal performance are affected by interaction with other subsystems.

Here, we use techniques from information theory and statistical mechanics to show that subsystem performance and interactions can be concretely cast in terms of “stress” and “strain” from materials physics. We illustrate this behavior in design problems that can be cast as arrangement problems. Arrangement problems arise in design in a wide range of disciplines, including at several scales in electronics,[10] as well as in distribution logistics [11] and facility layout.[12] Here, we focus on arrangement problems that arise in naval architecture.[13] Naval architecture, specifically that of warships or other multi-use vessels, provides an ideal case for understanding the role of subsystem behavior in complex engineering design. Ships incorporate several competing design pressures,[5, 14] they require design specifications at several levels of detail,[15] and costs frequently prevent prototype production.[16] Additionally, ship design has a need for design flexibility, i.e. it requires the consideration of nearly-

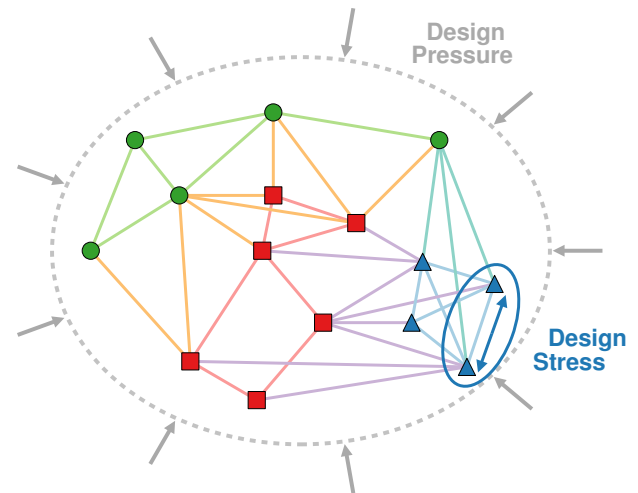


FIG. 1. **Schematic of the relationship between global design pressure and local design stress in a generic design problem.** A complex system (whole network) is divided into three subsystems (represented by green, red, and blue nodes). Design pressure is represented by the inward pointing grey arrows and applies to all parts of the system. Locally, the global design pressure manifests itself as design stress, here between two blue nodes.

redundant designs of comparable “cost” of the overall design objective. This type of design cannot be done via approaches that focus on finding individual designs, e.g. simulated annealing [17], that don’t capture entropic drives in design. We show that situating design problems in a more generic statistical physics framework facilitates the computation of *local* “design stress” that arises in subsystems from different competing *global* design pressures (see Fig. ?? for illustration). We demonstrate how global design pressures from the remainder of a system induce sub-optimal subsystem performance, which we quantify through Pareto frontiers computed using effective, or Landau,[18] free energies. Our approach draws on work on effective interactions in soft matter systems without a clear separation of scales [19–21] and on statistical mechanics based approaches for materials design,[22, 23]

which we apply here at the level of systems. Using this “systems physics” approach, we compute free energies for sample systems and show how the effects of competition between design pressures drive subsystem designs into distinct classes. We also use the same method to show that it is possible to determine likely arrangements of functional units, and routings between them, independently. Our approach gives new concrete, quantitative understanding of how competing design pressures affect subsystem design in complex naval systems. Our approach can be straightforwardly generalized to other classes of design problems involving complex couplings between interconnected systems.

## II. SYSTEMS PHYSICS FRAMEWORK

We seek a framework for studying tradeoffs in design problems. To do so, we begin from the fact that many classes of design problems can be cast in the form of a network of functional components.[13, 24] Different candidate design realizations arise from different intrinsic properties of the functional units, the topology of the network of functional connections and, possibly, the spatial embedding of the functional network. For many real-world design problems this results in a combinatorially large space of feasible design solutions.[24–26] The structure of design space determines the form of tradeoffs between design considerations.

To study how the structure of design space encodes tradeoffs, we consider a combinatorially large set of feasible designs ( $\{\sigma\}$ ) and a set of design objectives ( $\{\mathcal{O}_i\}$ ). A powerful approach to the design of complex engineering systems, known as Set-Based Design,[2–5] involves finding candidate sets of feasible designs, as opposed to focusing on a singular optimal design.[7] Different design objectives select different corners of the full design space into the candidate set. Given the full design space and a set of specified average outcomes for the design objectives ( $\{\langle\mathcal{O}_i\rangle\}$ ), an important task is to determine the probability ( $p_\sigma$ ) that a given design  $\sigma$  would be selected for inclusion in the set of candidate designs.

To construct a set of candidate designs with average outcomes  $\{\langle\mathcal{O}_i\rangle\}$  for the design objectives, information theory [27, 28] indicates that the least-biased estimate of  $p_\sigma$  is given by maximizing the functional

$$S = - \sum_{\sigma} p_{\sigma} \ln p_{\sigma} - \sum_i \lambda_i \left( \sum_{\sigma} p_{\sigma} \mathcal{O}_i(\sigma) - \langle \mathcal{O}_i \rangle \right), \quad (1)$$

with respect to  $p_\sigma$ , where  $\lambda_i$  are Lagrange multipliers enforcing the constraint on candidate designs. Carrying out the maximization gives

$$p_{\sigma} = \frac{1}{\mathcal{Z}} e^{-\sum_i \lambda_i \mathcal{O}_i(\sigma)}, \quad (2)$$

where  $\mathcal{Z}$  is a normalization constant. In principle, further algebraic manipulation could determine the  $\lambda_i$  and yield a precise form for  $p_\sigma$ . That form of  $p_\sigma$  would answer the question of *what* designs are likely to be selected. *Why* certain design classes are likely to be selected, however, presents an

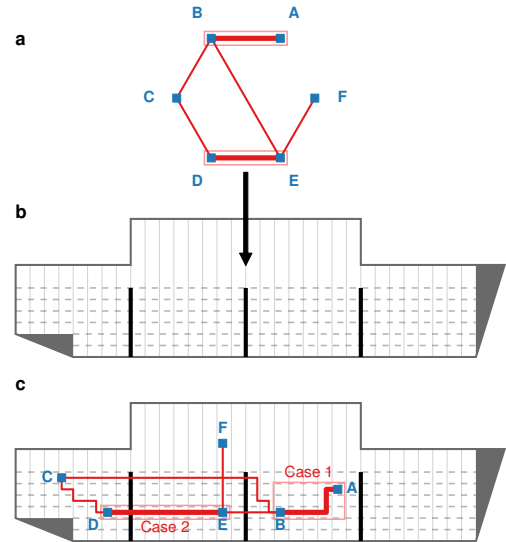


FIG. 2. **Illustration of the model for arrangement problems.** The functional network (a) is embedded into an inhomogeneous space (b), here a ship hull. Spatial embeddings (c) require routings between connections, with two generic cases. Case 1, routings that are not affected by features of the embedding space, is described in Figs. 2 and 3. Case 2, routings that are affected by features of the embedding space, here bulkheads, is described in Figs. 4-6.

equally important question. Answering this question is important in untangling the dependence of specific design solutions on overall design priorities. To answer the “why?” question, we note that  $p_\sigma$  has the form of Boltzmann weight in statistical physics. Using the statistical physics approach takes us from Eq. (2) to the so-called partition function

$$\mathcal{Z} = e^{-\sum_i \lambda_i \mathcal{O}_i(\sigma)}, \quad (3)$$

in which each  $\lambda_i$  quantifies the “design pressure” of meeting corresponding design objective  $\mathcal{O}_i$ . By specifying how the variable design pressure affects the determination of candidate designs, the partition function provides a means to determine why candidate designs are candidates. To concretely demonstrate the power of this approach for general design problems, we use a specific problem from naval architecture. However, this approach generalizes straightforwardly to other problem classes by appropriate selection of candidate designs ( $\sigma$ ) and design objectives ( $\mathcal{O}_i$ ).

## III. ARRANGEMENT PROBLEM MODEL

We consider the spatial embedding of a subsystem of the overall functional network that contains only two units and a single functional connection. In both cases we choose a subsystem at random among two possible cases that differ by whether the embedding of the remainder of the functional network localizes the subsystem in a homogeneous space (Case

1), or a space that is structured by the remaining ship design (Case 2). See Fig. 2 for an illustration. We show below that Case 1 exhibits behavior that results from trade-offs between considerations of cost and flexibility, and Case 2 exhibits behavior that results from trade-offs between considerations of cost, flexibility, and performance.

In both cases, the monetary cost expended on routing a connection between units ( $E$ ) is given by the ‘‘Manhattan’’ distance (the sum of horizontal and vertical steps) of a minimal path between the units at some cost per unit length  $C$ . The objective for units separated by some relative  $\Delta x$  and  $\Delta y$  is

$$\mathcal{O}_1 \equiv E = C(\Delta x + \Delta y), \quad (4)$$

and we quantify the design pressure for cost through  $\lambda_1 \equiv 1/T$  where  $T$  is interpreted as a ‘‘cost tolerance’’. Low cost tolerance means that the design pressure to minimize costs is strong, which should lead to a preference for low cost designs. Increasing cost tolerance weakens the design pressure to minimize costs. Note that the limit of  $T \rightarrow \infty$  represents complete indifference to cost as a design decision factor, rather than a preference for high cost. In statistical physics terms,  $E$  plays the role of energy,  $T$  plays the role of temperature. In addition, distinct routings and overall displacements of the units contribute entropy, a measure of the flexibility to realize distinct designs at fixed cost.

In addition, Case 2 models the performance penalty associated with routing functional connections through the bulkhead. We do so with the objective

$$\mathcal{O}_2 \equiv B, \quad (5)$$

which takes the value 1 if a routing penetrates the bulkhead and 0 if it does not. We represent the penalty for bulkhead penetration by  $\lambda_2 \equiv \gamma$ .

In both cases we use statistical physics to extract design information. Constitutive relations or ‘‘equations of state’’, evaluated via the expression

$$\langle \mathcal{O}_i \rangle = -\frac{\partial \ln \mathcal{Z}}{\partial \lambda_i}, \quad (6)$$

quantify how outcomes for design objectives are determined by design pressure. In the specific case we consider here, fixing the design pressures through  $T$  and  $\gamma$  yields expected outcomes for  $\langle E \rangle$  and  $\langle B \rangle$ , which indicate expected costs and likelihood of bulkhead penetration, respectively. Likewise, the sensitivity of design outcomes to changes in design pressure is described by ‘‘susceptibilities’’ that can be evaluated by further differentiation. The magnitude of susceptibility is directly related to the magnitude of fluctuations about the average design objective (see SM for more information). We also evaluate the likely design outcomes for specific design features  $S_j$

$$\langle S_j \rangle = \frac{1}{\mathcal{Z}} \sum_{\sigma} S_j(\sigma) e^{-\sum_i \lambda_i \mathcal{O}_i(\sigma)}. \quad (7)$$

Finally, effective, or Landau, free energies  $F$  for different system elements (e.g. unit locations, routing locations) can be

computed as

$$e^{-F(S_j)} \propto \sum_{\sigma} \delta(S_j(\sigma) - S_j) e^{-\sum_i \lambda_i \mathcal{O}_i(\sigma)}, \quad (8)$$

and represent the change in the overall design objective resulting from the competition between the design pressures. Minimal free energy corresponds to the optimal design, whereas free energy isosurfaces represent non-optimal Pareto frontiers. Differentiating the free energy ( $-\nabla F$ ) yields a ‘‘design stress’’, which quantifies how overall, global design pressure is distributed locally among design elements in the subsystem. Similarly, ‘‘design strain’’ in a subsystem expresses the displacement of subsystem units or routings from optimality due to stress between subsystem and whole system design pressure. Details of analytic and numerical computations that yield these quantities for our model systems are described in SM.

## IV. RESULTS

We consider the spatial embedding of a subsystem of the overall functional network that contains only two units and a single functional connection. In both cases we choose a subsystem at random among two possible cases that differ by whether the embedding of the remainder of the functional network localizes the subsystem in a homogeneous space (Case 1), or a space that is structured by the remaining ship design (Case 2). See Fig. 2 for an illustration. We will show below that Case 1 exhibits behavior that results from trade-offs between considerations of cost and flexibility, and Case 2 exhibits behavior that results from trade-offs between considerations of cost, flexibility, and performance.

### A. Case 1, Homogeneous Embeddings: Cost/Flexibility Trade-off

We consider the homogeneous embedding of a subsystem with two units, labeled  $A$  and  $B$ , within a homogeneous region of space, here a single watertight compartment (illustrated schematically in Fig. 2c). The location of  $A$  and  $B$  within the compartment, and the routing of a functional connection between them, leads, in our model system, to a trade-off between cost expenditure,  $E$ , and flexibility, measured by the routing entropy. The optimal design of this subsystem is determined by the relative importance of cost and flexibility, which we parametrize through the cost tolerance  $T$ . In Fig. 3a we illustrate example schematic embeddings of the subsystem of interest into a region of space of size  $L \times L$ . We study examples in which the subsystem is highly localized ( $L = 10$ ) and delocalized ( $L = 100$ ) in Fig. 3b-d. For both values of  $L$  we study ensembles of design solutions at a series of values for cost tolerance.

For  $L = 10$ , we find that there is a slowly varying, monotonic increase in average cost with increasing cost tolerance (Fig. 3b, blue curve). However, for  $L = 100$ , where the subsystem embedding is less constrained by the remainder of

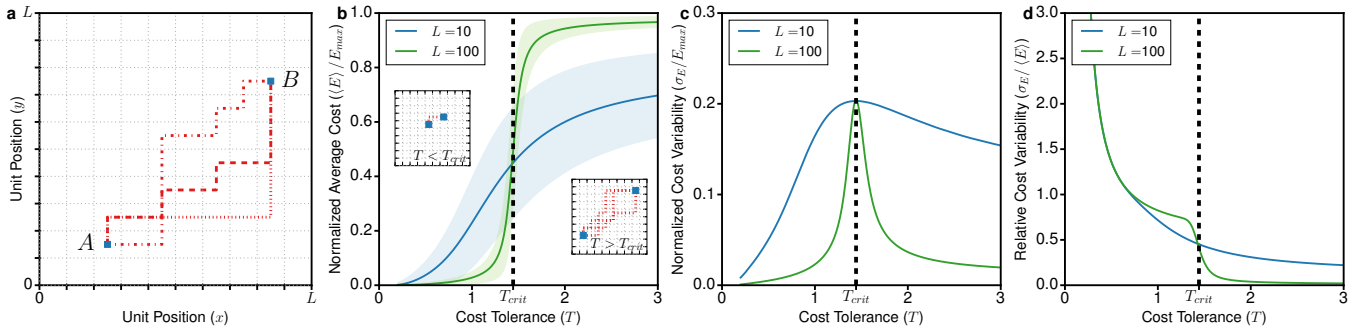


FIG. 3. (a) Example unit positions and routings for spatially homogeneous subsystem embeddings (Case 1, see Fig. 2). Blue markers indicate unit positions, red lines indicate possible routings. (b) Equation of state relating cost tolerance ( $T$ ) and average cost ( $\langle E \rangle$ , in currency) normalized by maximum possible cost expended ( $E_{\max}$ ) for subsystems localized in an  $L \times L$  region of a ship ( $L = 10$  blue curve;  $L = 100$  green curve). Shaded areas indicate cost variability. Inset images illustrate typical design realizations below (condensed) and above (separated)  $T_{\text{crit}} = 1/\ln(2)$ . (c) Cost variability ( $\sigma_E$ , a susceptibility) normalized by maximum possible expenditure as a function of cost tolerance. The peak at  $T_{\text{crit}}$  for a finite sized system ( $L = 100$ ) would correspond to a phase transition in the thermodynamic limit. (d) Cost variability normalized by average expenditure as a function of cost tolerance. Data indicate that for both large and small systems relative cost variability is large for low average cost designs.

the network, we find a sharp increase in cost around  $T_{\text{crit}} = C/\ln 2$  (Fig. 3b, green curve). This sharp increase in cost is reminiscent of a phase transition in physical systems, and we find that the amount of absolute cost uncertainty across feasible solutions (Fig. 3c; akin to a susceptibility for cost) has a peak at  $T_{\text{crit}}$ . For  $L = 100$ , when the subsystem is less constrained, the absolute cost uncertainty is low at both low and high cost tolerance, indicating that in those regimes routings between unit pairs are almost always cheap, or almost always expensive relative to possible maximum cost. For  $L = 10$ , when the subsystem is more tightly constrained, the absolute cost uncertainty is large over a broad range of cost tolerances.

However, when measured relative to average cost, we find that cost uncertainty is large for both  $L = 10$  and  $L = 100$  in the limit of low cost tolerance. Fig. 3d shows that relative cost uncertainty diverges as cost tolerance goes to zero. This result means that even though, as expected, low cost tolerance leads to low cost designs for the subsystem of interest, possible design outcomes show uncertainty of 100% or more in terms of average cost. Though this effect might not be a large design concern if it occurred only in the subsystem of interest, we note that our choice of subsystem was arbitrary, so that every subsystem in the network should exhibit this effect. A cascade of such occurrences throughout a large functional network in a complex product, such as a ship, would lead to large macroscopic fluctuations in cost of the overall design.

For  $L = 100$ , Fig. 3d indicates that as the cost tolerance increases across the critical value, there is a sharp drop in the cost uncertainty relative to average cost, that is driven by the sharp increase in average cost seen in Fig. 3b. This indicates that above the critical cost tolerance candidate designs are high cost, but show relatively small cost uncertainty. Taken together, the features of the relative cost uncertainty curve indicate a fundamental trade-off: tight cost constraints lead to wild relative cost uncertainty, whereas low relative cost uncertainty can only be achieved at large cost.

To make the origin of these behaviors more concrete, in

Fig. 4 we fix the position of one of the units to be the origin, and examine how the design pressures from cost (Fig. 4a) and flexibility (Fig. 4b) influence the  $(x, y)$  location of the second unit. For the case of  $L = 30$ , we plot one quadrant, the other quadrants being related by symmetry. Arrows indicate the relative magnitude and direction of stress that each different form of design pressure induces on the location of the second unit. Comparing Fig. 4 panels a and b shows that cost and flexibility pressures act in different directions with cost driving the units closer together and flexibility driving them further apart. The balance between these forces is determined by the cost tolerance, and leads to qualitatively different outcomes depending on this value, which can be seen in the Pareto frontiers plotted in Fig. 4c-f. For physics readers, we note that Pareto frontiers correspond to isosurfaces of the Landau free energy (see, e.g., Ref. [18]) for unit locations. We plot Pareto frontiers describing the deviation from the optimal overall objective at a series of cost tolerances. The reason for considering non-optimal solutions is that any subsystem is only part of the overall design, and we do not expect that, in general, overall optimal designs will correspond to optimal outcomes for all subsystems. Non-optimal Pareto frontiers provide a means of communicating how design pressure from the rest of the functional network could be expected to influence the behavior of a subsystem.

When we compute the corresponding Pareto frontiers, we find that at low cost tolerance ( $T = 0.1$ ; Fig. 4c), units are condensed, since the behavior is dominated by cost minimization, which is characterized by Pareto frontiers with constant  $x + y$  in the limit of  $T = 0$ . Increasing cost tolerance alters the balance between cost and flexibility. Even below the critical tolerance ( $T = 1.3$ ; Fig. 4d), this causes a change in shape in the Pareto frontiers. At the critical cost tolerance ( $T = T_{\text{crit}}$ ; Fig. 4e) Pareto frontiers more closely resemble surfaces with constant  $x - y$  rather than  $x + y$  as we found at low temperature. Above the critical cost tolerance ( $T = 2.0$ ; Fig. 4f), Pareto frontiers reverse their order with low free energy locations for the location of the second unit forced to the

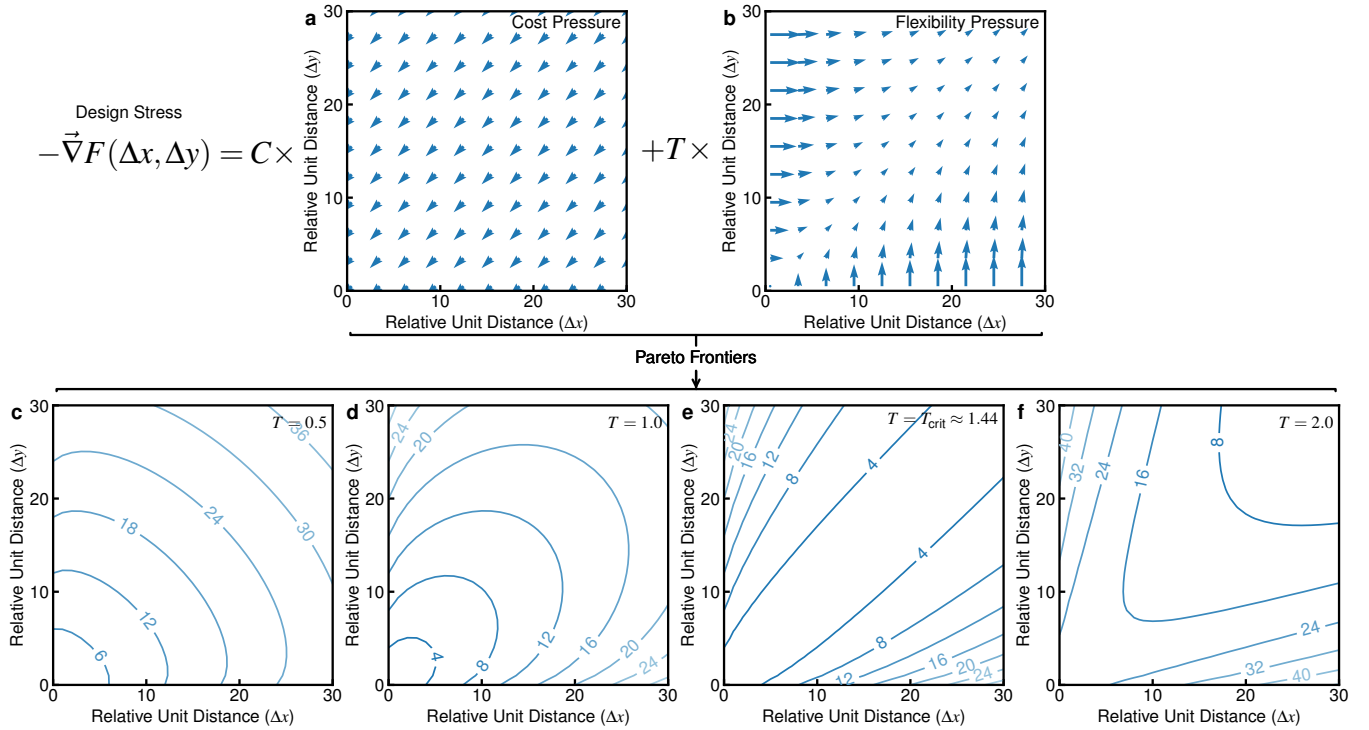


FIG. 4. Pressure from overall design objectives induces stress on subsystem design elements. For spatially homogeneous subsystem embeddings (Case 1, see Fig. 2) design stress can be decomposed into contributions from cost pressure (panel a) and flexibility pressure (panel b). Depending on the relative strength of the design pressures, the different phase behaviors in Fig. 3 originate from underlying subsystem effects, illustrated in panels c-f. Panels c-f plot Pareto frontiers (Landau free energy isosurfaces) that indicate equivalent, suboptimal subsystem designs that could arise if the subsystem design was forced to sacrifice performance to the remainder of the system. At low cost tolerance ( $T = 0.5$  c;  $T = 1.0$  d) units are preferentially condensed. At high cost tolerance ( $T = 2.0$  f) units are preferentially separated. At the critical cost tolerance ( $T = T_{\text{crit}} = 1/\ln 2$ ) there is no preferred separation distance.

boundary.

### B. Case 2, Inhomogeneous Embeddings: Cost/Flexibility/Performance Trade-offs

We next consider the additional design pressure that arises from an inhomogeneous embedding space. For concreteness, we represent this as a bulkhead within the ship hull. Bulkheads are features designed to prevent water that enters the hull through a breach from filling all parts of hull and sinking the ship. Routings through a bulkhead are expensive and also can reduce its effectiveness, and thus overall ship performance. Hence, additional performance pressure arises in the case that elements of a subsystem are located in different bulkhead compartments (schematic illustration in Fig. 2c). We parametrize it with bulkhead penalty  $\gamma$ , acting as the second design pressure in the system. Again, from a large functional network we randomly choose a subsystem comprised by a pair of units with a single functional connection. However, we assume that the connections between the subsystem of interest and the remainder of the functional network drive the location of one unit to be on one side of the bulkhead and the other unit to be on the opposite side. We allow two types of routings between the units to study their trade-off: one routes along the

shortest path through the bulkhead and suffers the penalty  $\gamma$ ; the other routes along the shortest path around the bulkhead, with no penalty. For concreteness we give results for systems of fixed size ( $20 \times 20$  with a vertical bulkhead in the middle) which are representative of the general behaviors we observe. See SM for results for other system sizes.

Compared with Case 1, breaking spatial homogeneity makes the relationship between route paths and unit locations more complicated. This complication arises because routings now couple to both unit positions and geometric features. Because of this, we study unit positioning and routing separately. As in Case 1, we compute Pareto frontiers via Landau free energies, but in this case we do so by integrating out the degrees of freedom of units and routings separately. Fig. 5 shows Pareto frontiers for unit routing positions as a function of cost tolerance for bulkheads with representative high ( $\gamma = 8$ , panels a-h) and low ( $\gamma = 2$ , panels i-p) bulkhead penalty. The difference of  $\Delta\gamma = 6$  between the two values implies that the relative statistical weight of routing through the bulkhead changes roughly by a factor of  $e^6 \sim 400$ , and the effects on node positioning are immediately visually apparent. Also apparent is the effect of  $\Delta\gamma$  on design performance, characterized by the  $\langle B \rangle$ , i.e. the fraction of all designs that route through the bulkhead. See SM for computation details.

At high bulkhead penalty ( $\gamma = 8$ ), and low cost tolerance

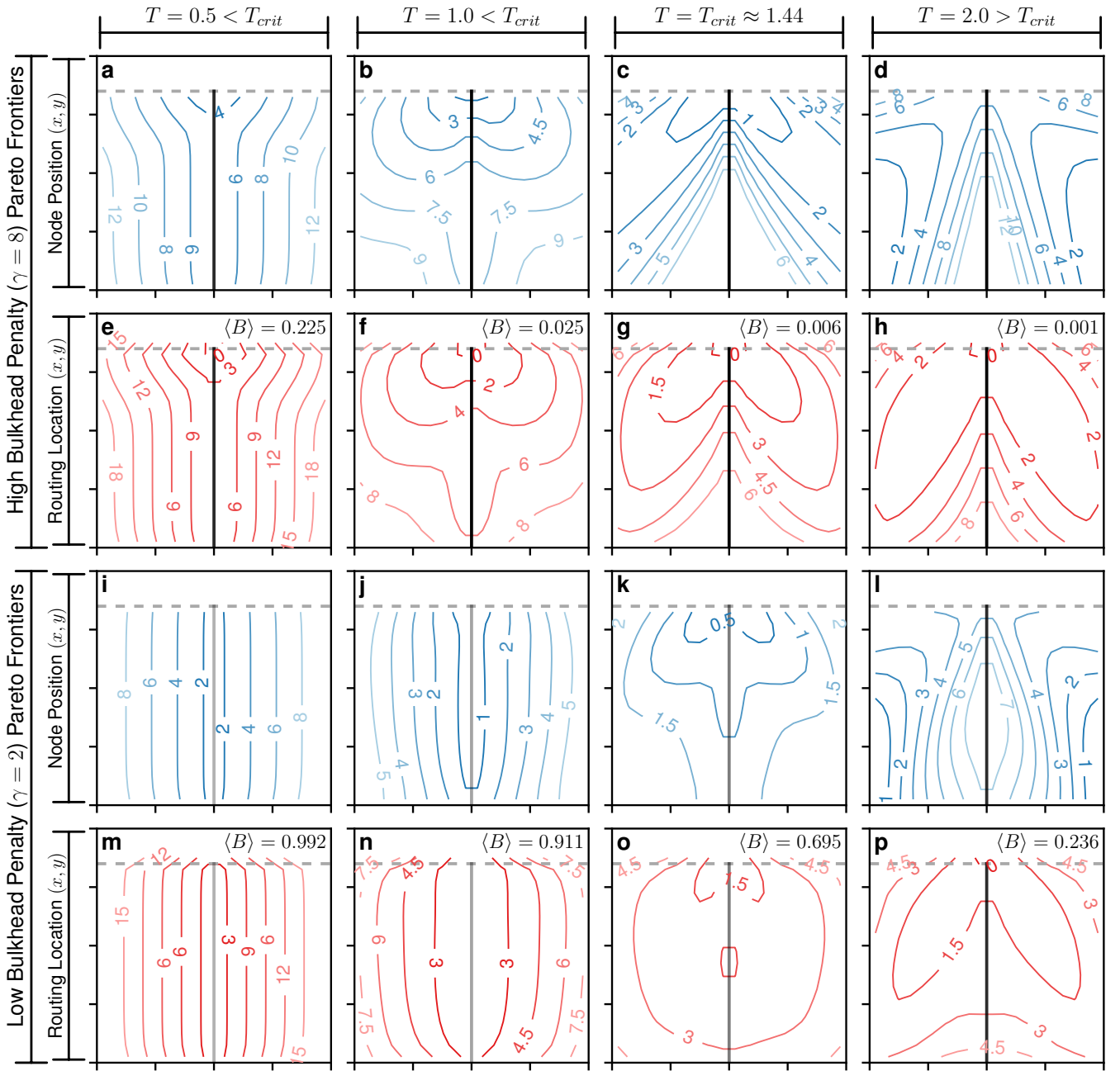


FIG. 5. Pareto frontiers (Landau free energy isosurfaces) for unit and routing locations for spatially inhomogeneous subsystem embeddings (Case 2, see Fig. 2) for different cost tolerances  $T$  ( $T = 0.5$  first column,  $T = 1.0$  second column,  $T = T_{\text{crit}}$  third column,  $T = 2.0$  fourth column) and performance penalties for bulkhead penetration ( $\gamma = 8$  top two rows,  $\gamma = 2$  bottom two rows). Blue curves indicate unit positions, normalized so that most favorable unit locations have value 0, with increasing values indicating the loss in subsystem objective in units of the cost tolerance. Red curves indicate routing locations, normalized so that locations through which connections route with absolute certainty have value 0, and increasing values indicate the reduction in subsystem objective of routing through a given location in units of cost tolerance.

( $T = 0.5$ ) Pareto frontiers for unit locations (Fig. 5a) and routing (Fig. 5e) both indicate strong coupling to the top of the bulkhead. Results for increased cost tolerance ( $T = 1.0$ ) that is still below  $T_{\text{crit}}$  indicate that unit locations are less strongly coupled to the bulkhead (Fig. 5b). Comparison with results for routing (Fig. 5f) indicate that this coincides with a

drop in fraction of designs that route through the bulkhead by nearly an order of magnitude ( $\langle B \rangle = 0.025$  at  $T = 1.0$ , c.f.  $\langle B \rangle = 0.225$  at  $T = 0.5$ ), and though routes remain strongly localized at the top of the barrier, Pareto frontiers at equivalent objective cost (free energy) are further from the bulkhead. These trends continue through  $T_{\text{crit}}$  (Fig. 5c,g). How-

ever, above  $T_{\text{crit}}$  ( $T = 2.0$ ) Fig. 5d we observe that although the units delocalize from the bulkhead (Fig. 5d), the routings remain strongly coupled to the top of the bulkhead, and the probability that a design routes through the bulkhead drops to  $\langle B \rangle = 0.001$ . Comparing unit locations (Fig. 5a-c) and routing locations (Fig. 5e-g) indicates that at or below  $T_{\text{crit}}$  unit locations are correlated with routing locations. However, above  $T_{\text{crit}}$  (Fig. 5d,h) indicates that most probable unit locations do not correspond to most probable routing locations.

We contrast the above results at high bulkhead penalty ( $\gamma = 8$ , Fig. 5a-h) with low bulkhead penalty ( $\gamma = 2$ , Fig. 5i-p). At low cost tolerance ( $T = 0.5$ ) we see that relaxing the bulkhead penalty still causes the unit positions to localize near the bulkhead (Fig. 5e) but the units no longer localize near the top of the bulkhead as they did at high bulkhead penalty (Fig. 5a). Likewise, routings no longer localize near the top of the bulkhead (Fig. 5m), but follow the unit locations and pierce the bulkhead with high probability ( $\langle B \rangle = 0.992$ ). At increased cost tolerance ( $T = 1.0, T_{\text{crit}}$ ) the localization at the top of the bulkhead appears again (Fig. 5j-k,n-o). At high cost tolerance  $T = 2.0$  the units again delocalize from the bulkhead (Fig. 5l,p) and the cases  $\gamma = 2$  and  $\gamma = 8$  start looking very similar.

To further understand the competing design pressures of cost, flexibility, and performance, we compute design stress in unit positioning (see Fig. 6). At a given unit position (corresponding to “strain” in the language of materials science) design stress indicates the magnitude and direction in which changing the placement of the unit would lead to the greatest decrease in the overall objective cost for the subsystem. We find that at low cost tolerance ( $T = 0.5$ , Fig. 6a,e), design stress is directed primarily toward the bulkhead, with discernible stress toward the top of the compartment for high cost penalty. An increase in cost tolerance ( $T = 1.0$ , Fig. 6b,f) leads to similar design stress at low bulkhead penalty (Fig. 6f) but a more intricate pattern of stress at high bulkhead penalty (Fig. 6b) that includes regions with stress toward and away from the both the bulkhead and the top of the compartment. Similarly, complex patterns of stress occur at both low and high bulkhead penalty at  $T_{\text{crit}}$  (Fig. 6c,g). At high cost tolerance ( $T = 2.0$ , Fig. 6d,h), the pattern of design stress is predominantly away from the bulkhead.

The behaviors we find that arise from the competition between cost, flexibility, and performance design pressures can be classified qualitatively according to the phase diagram in Fig. 7. In Fig. 7 we show, schematically, the effects of bulkhead penalty  $\gamma$  and cost tolerance  $T$  on bulkhead penetration (a) and relative unit distance (b). The combination of these effects also results in a complicated emergent relationship between the vertical positions of the units (c). To provide a more concrete and quantitative example, panels (d) and (e) show respectively the bulkhead penetration fraction and the correlation in vertical node positions for the same system of size  $L = 20$ .

## V. CONCLUSION

We developed a general, statistical physics framework for analyzing complex design problems. We demonstrated the application of this framework to characterizing tradeoffs between competing design pressures. For concreteness, we studied trade-offs between competing design pressures of cost, flexibility, and performance in arrangement problems from naval architecture design. We analyzed ship models by applying physics principles at the systems-level and found a rich pattern of behavior. We gave an explicit formulation of Pareto frontiers in terms of isosurfaces of Landau free energy, and computed “design stress” induced by sub-optimal subsystem embedding. Our framework recasts common design challenges in terms of the well-understood concepts of pressure, stress and strain. We find that these concepts, which are typically used to characterize the behavior of materials, also provide a means of characterizing system-level behavior.

Our approach opens new avenues for addressing design challenges that arise in complex systems. Our framing of system design in terms of statistical mechanics has some technical overlap with optimization approaches based on simulated annealing.[17] Simulated annealing invokes thermodynamics by using a fictitious Hamiltonian cooled *in silico* to zero temperature to find the global minimum of an objective function. Our approach with minimally biased probability distributions, though derived from information theory, is mathematically equivalent to a fictitious Hamiltonian held at a constant *finite* temperature. Maintaining finite temperature highlights the role of design pressures that arise from flexibility and become relevant in combinatorially large optimization spaces, and in early stage design.[6] We found this approach gives important information about the systems of interest: the separation of subsystem designs into different architecture classes; knowledge about where paths between units are likely to route even if the unit locations are not specified, and vice versa; knowledge about cost variability for low and high subsystem cost tolerance; understanding of how different design objectives create design stress on subsystems. All of these forms of knowledge are crucial in the early design stages of a broad class of complex design problems.

Finally, physics concepts and principles are typically used to understand the behavior of a part of a larger system. E.g. for a ship it is common to: use the physics of electromagnetism to understand the function of a radar; use materials physics to understand the properties of a hull; use solid state physics to understand the properties of electronics; use hydrodynamics to understand the interaction of a hull with water; use thermodynamics to understand the function of an engine. Here, without explicit reference to the underlying physical nature of the component systems, we showed that familiar physics concepts, such as pressure, stress, and strain, via the principles of statistical mechanics, give new insight into the architecture of a ship as a whole. Our focus on an established,[13] minimal model of ship design was motivated both by pressing challenges in naval architecture, and by the goal of providing a concrete, self-contained example of our approach. However, our “systems physics” approach gener-

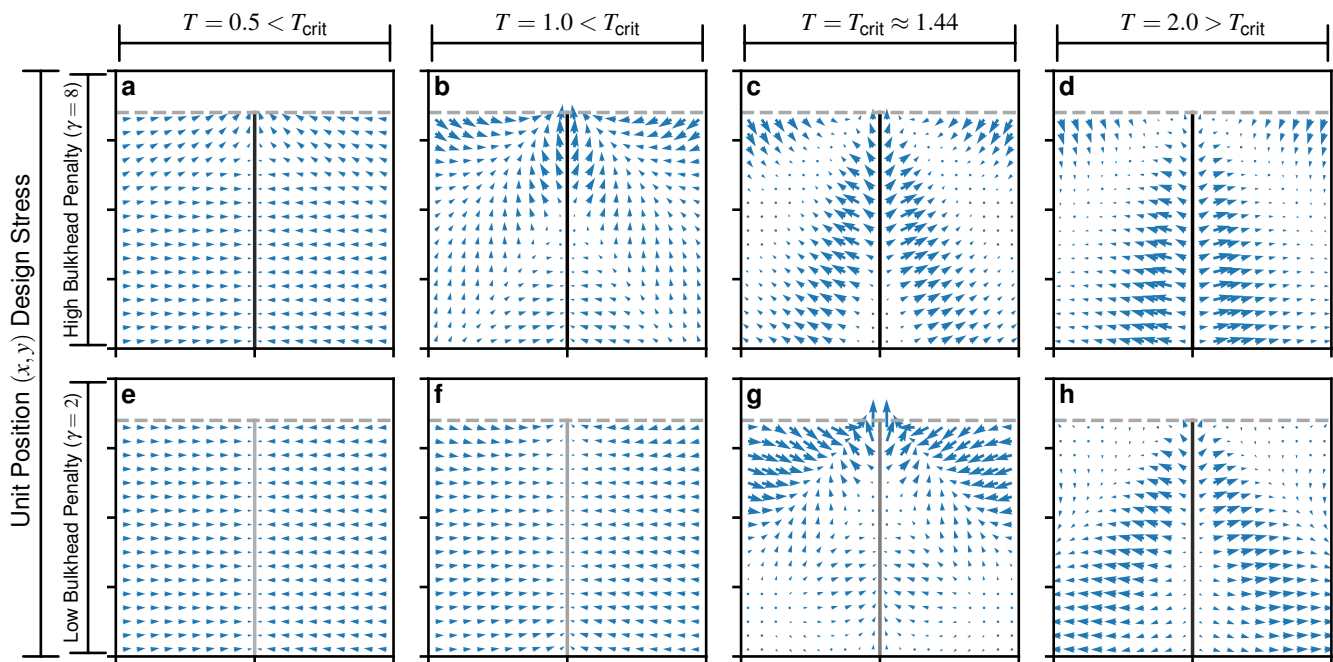


FIG. 6. Design stress for unit locations in spatially inhomogeneous subsystem embeddings (Case 2, see Fig. 2) for different cost tolerances  $T$  ( $T = 0.5$  first column,  $T = 1.0$  second column,  $T = T_{\text{crit}}$  third column,  $T = 2.0$  fourth column) and performance penalties for bulkhead penetration ( $\gamma = 8$  top row,  $\gamma = 2$  bottom row). Plots indicate that if a unit was sited at the origin of an arrow in response to whole system design pressure, design pressure acting on the subsystem alone would drive the unit in the direction of the arrow, with a strength proportional to the length of the arrow.

alizes straightforwardly in several respects: to more detailed models of naval architecture, to subsystems with more units, and more complex functional connections, and, most importantly, and to other classes of systems-level design problems. Systems-level applications of physics have led to constructive engagements between physics and economics,[29, 30] network science,[31, 32] and epidemiology.[33, 34] We believe the present systems-level application of physics will lead to a similar constructive engagement with design problems in a

wide variety of domains.

We thank B. Ames, L. Conway, and M. Newman for several helpful discussions. This work was supported by the U.S. Office of Naval Research Grant Nos. N00014-17-1-2491 and N00014-15-1-2752 as well as Government support under contract FA9550-11-C0028 and awarded by the Department of Defense, Air Force Office of Scientific Research, National Defense Science and Engineering Graduate (NDSEG) Fellowship, 32 CFR 168a.

- 
- [1] B. S. Blanchard and W. J. Fabrycky, *Systems engineering and analysis*, Vol. 4 (Prentice Hall, Englewood Cliffs, NJ, 1990).
- [2] J. K. Liker, *The Toyota Way* (McGraw-Hill, New York, 2004).
- [3] J. M. Morgan and J. K. Liker, *The Toyota product development system*, Vol. 13533 (Productivity Press, New York, 2006).
- [4] J. I. Bernstein, *Design methods in the aerospace industry: looking for evidence of set-based practices*, Ph.D. thesis, Massachusetts Institute of Technology (1998).
- [5] D. J. Singer, N. Doerry, and M. E. Buckley, *Naval Engineers Journal* **121**, 31 (2009).
- [6] J. Chalfant, *Proceedings of the IEEE* **103**, 2252 (2015).
- [7] J. H. Evans, *Naval Engineers Journal* **71**, 671 (1959).
- [8] J. Manyika, J. Sinclair, R. Dobbs, G. Strube, L. Rassey, J. Mischke, J. Remes, C. Roxburgh, K. George, D. O'Halloran, and S. Ramaswamy, *Manufacturing the future: The next era of global growth and innovation* (McKinsey Global Institute, 2012).
- [9] "Manufacturing industry: Politicians cannot bring back old-fashioned factory jobs," *The Economist* (2017).
- [10] M. C. Dorneich and N. V. Sahinidis, *Engineering Optimization+ A35* **25**, 131 (1995).
- [11] C. H. Aikens, *European journal of operational research* **22**, 263 (1985).
- [12] A. Drira, H. Pierreval, and S. Hajri-Gabouj, *Annual Reviews in Control* **31**, 255 (2007).
- [13] C. P. Shields, D. T. Rigterink, and D. J. Singer, *Ocean Engineering* **135**, 236 (2017).
- [14] A. Brown and J. Salcedo, *Naval Engineers Journal* **115**, 49 (2003).
- [15] D. J. Andrews, *Proc. Roy. Soc. London A* **468**, 891 (2012).
- [16] J. M. Ross, *COMPIT* **4**, 98 (2004).
- [17] S. Kirkpatrick, C. D. Gelatt, and M. P. Vecchi, *Science* **220**, 671 (1983).
- [18] N. Goldenfeld, *Lectures on phase transitions and the renormal-*



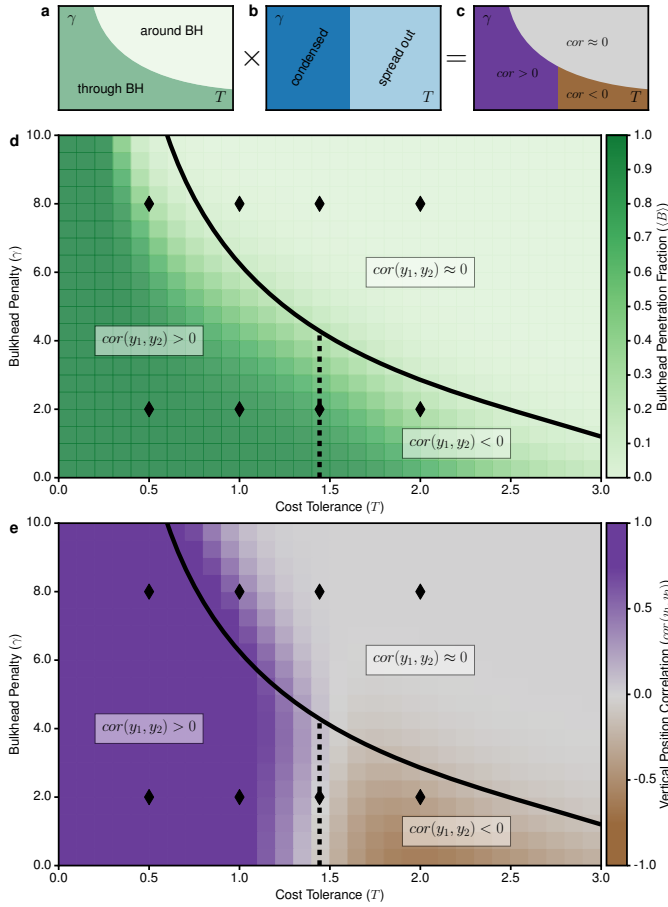


FIG. 7. Phase diagram for spatially inhomogeneous subsystem embeddings (Case 2, see Fig. 2), summarizing effects of performance penalties associated with bulkhead penetration ( $\gamma$ ) and cost tolerance ( $T$ ). (a) Schematic illustration of effects of  $T$  and  $\gamma$  on bulkhead penetration (performance proxy) for arbitrary subsystem localization. (b) Schematic illustration of effects of  $T$  and  $\gamma$  on unit separation (cost proxy) for arbitrary subsystem localization. (c) Schematic illustration of combination of bulkhead penetration (performance proxy) and unit separation (cost proxy) on vertical correlation in unit layout (architecture-class proxy) for arbitrary subsystem localization. (d) Quantitative phase plot for subsystem localization of fixed size  $L = 20$ . Green shade indicates average system performance (bulkhead penetration probability). (e) Quantitative phase plot for vertical correlation in unit layout (architecture-class proxy). Markers in (d-e) indicate  $T, \gamma$  values corresponding to plots in Figs. 5 and 6.

ization group (Addison-Wesley, Reading MA, 1992).

- [19] C. N. Likos, *Physics Reports* **348**, 267 (2001).  
 [20] G. van Anders, D. Klotsa, N. K. Ahmed, M. Engel, and S. C. Glotzer, *Proc. Natl. Acad. Sci. U.S.A.* **111**, E4812 (2014), arXiv:1309.1187 [cond-mat.soft].  
 [21] G. van Anders, N. K. Ahmed, R. Smith, M. Engel, and S. C. Glotzer, *ACS Nano* **8**, 931 (2014), arXiv:1304.7545 [cond-mat.soft].  
 [22] G. van Anders, D. Klotsa, A. S. Karas, P. M. Dodd, and S. C. Glotzer, *ACS Nano* **9**, 9542 (2015), arXiv:1507.04960 [cond-mat.soft].  
 [23] M. Z. Miskin, G. Khaira, J. J. de Pablo, and H. M. Jaeger, *Proc. Natl. Acad. Sci. U.S.A.* **113**, 34 (2016).  
 [24] C. Mead and L. Conway, *Introduction to VLSI systems*, Vol. 1080 (Addison-Wesley Reading, MA, 1980).  
 [25] M. S. Daskin, *Network and discrete location: models, algorithms, and applications* (John Wiley & Sons, 2011).  
 [26] C. P. F. Shields, M. J. Sypniewski, and D. J. Singer, in *Proceedings of the 13th International Symposium on PRACTical Design of Ships and Other Floating Structures (PRADS' 2016)*, edited by U. Nielsen and J. Jensen (Technical University of Denmark (DTU), 2016).  
 [27] C. Shannon, *Bell Syst. Tech. J.* **27**, 379 (1948).  
 [28] E. T. Jaynes, *Phys. Rev.* **106**, 620 (1957).  
 [29] R. N. Mantegna and H. E. Stanley, *Nature* **376**, 46 (1995).  
 [30] R. N. Mantegna and H. E. Stanley, *Introduction to econophysics: correlations and complexity in finance* (Cambridge University Press, 1999).  
 [31] R. Albert and A.-L. Barabási, *Rev. Mod. Phys.* **74**, 47 (2002).  
 [32] M. Newman, A.-L. Barabási, and D. J. Watts, *The Structure and Dynamics of Networks* (Princeton University Press, 2006).  
 [33] R. Pastor-Satorras and A. Vespignani, *Phys. Rev. Lett.* **86**, 3200 (2001).  
 [34] K.-I. Goh, M. E. Cusick, D. Valle, B. Childs, M. Vidal, and A.-L. Barabási, *Proc. Natl. Acad. Sci. U.S.A.* **104**, 8685 (2007).